PRAMANA
— journal of
physics

Vol. 79, No. 5
November 2012
pp. 1141–1167

Charged-lepton flavour physics

ANDREAS HOECKER
CERN, Meyrin, Geneva, Switzerland
E-mail: andreas.hoecker@cern.ch

Abstract. This write-up on a talk at the 2011 Lepton–Photon symposium in Mumbai, India, summarizes recent results in the charged-lepton flavour sector. Searches for charged-lepton flavour violation, lepton electric dipole moments and flavour-conserving CP violation are reviewed here. Recent progress in τ-lepton physics and in the Standard Model prediction of the muon anomalous magnetic moment is also discussed.

Keywords. Charged lepton interactions; leptons.

PACS Nos 13.60.−r; 14.65.−z; 13.15.+g

1. Introduction

The instability of the scalar sector of the Standard Model (SM) with respect to fermionic and bosonic loop corrections in the presence of an ultraviolet cut-off scale has been the driving motivation for the widespread expectation of TeV-scale new physics. Such new physics is in reach for discovery at the LHC which sets the current experimental energy frontier. Clean measurements in the charged-lepton flavour sector can also probe new physics at high scales, in fact, at mass scales up to hundreds of TeV and above, albeit the interpretation of a measurement in terms of mass scales is model-dependent. Such measurements often involve rare processes or small deviations in abundant processes (because they are scale-suppressed) and hence require large rates and high precision to be observable. The experiments performing these measurements operate at the intensity and precision frontier. Both, the energy and intensity/precision frontiers, are complementary domains of activity in modern particle physics research and so should be pursued in common.

Although some deviations between experiment and SM expectation exist in the charged flavour physics sector, none is presently significant enough to demonstrate evidence for new physics. It is nevertheless important to follow up on them. Just as important are the measurements for which, in our ignorance, one would have expected new physics to show up but none has been seen. Indeed, many of the models that have been developed to stabilize the Higgs boson sector, or that suggest alternatives to it, predict new

DOI: 10.1007/s12043-012-0422-2; ***e*Publication: 10 November 2012**

flavour-changing neutral currents, CP-violating phases, charged-lepton flavour violation, electric dipole moments, anomalous magnetic moments, contributions to electroweak precision observables, etc. Their non-observation strongly constrains these models, though – apart from very specific cases – does not exclude them. It does, however, affect their naturalness and the searches at the LHC, be they positive or not, will need to be scrutinized in view of the results from the precision measurements.

I review the following searches for charged-lepton flavour violation, lepton electric dipole moments and flavour-conserving CP violation. I also discuss recent progress in τ-lepton physics and in the SM prediction of the muon anomalous magnetic moment.

2. Charged-lepton flavour violation

Flavour violation involving charged leptons (LFV) belongs to the class of flavour-changing neutral currents (FCNC), which are suppressed at tree-level in the SM where they are mediated by γ and Z^0 bosons, but arise at loop level via weak charged currents mediated by the $W^\pm$ boson. The GIM mechanism [1] further suppresses loop-induced FCNC in the quark sector, so that FCNC effects are generally small in the SM. Rare FCNC processes such as $B_s^0 \to \mu\mu$ or $K_L^0 \to \pi^0\nu\bar{\nu}$, but also inclusive $b \to s$ transitions are therefore sensitive probes for new physics. The former mode is currently actively investigated at the LHC [2,3].

Because flavour violation requires mixing between families, charged LFV exactly vanishes in the SM for massless neutrinos. Extending the SM to include neutrino masses induces charged LFV via chirality flipping dipole amplitudes, which are however proportional to the fourth power in the ratio of neutrino mass splitting to W mass, giving, e.g., for the LFV decay $\mu \to e\gamma$ a branching fraction of roughly 10^{-54} [4], depending on the neutrino mixing angle θ_{13}. This is an unobservably tiny branching fraction so that the search for charged LFV probes new physics without SM contamination.

Experimentally, no evidence for charged LFV has been found so far. It is searched for in a variety of modes including the neutrinoless decays of a heavy lepton into a light one under emission of a radiative photon, or of a heavy lepton into three light ones. Using muonic atoms it is also possible to look for μ–e conversion in the electromagnetic field of the nucleus. Finally, τ leptons provide a profuse field of LFV searches with 48 different final states studied so far (see ref. [5] for a recent summary). A chronological overview of LFV limits is drawn in figure 1. It witnesses the many orders of magnitude improvement in the sensitivity obtained during half a century of LFV experiments. The tightest absolute limits on LFV effects are obtained in μ decays and μ–e conversion experiments. However, because different new physics phenomena induce different LFV effects, a quantitative comparison between the limits is model-dependent.

The absence of charged LFV had important consequences in the early days of particle physics when the concept of families was developed. Non-discovery of $\mu \to e\gamma$ and $\tau \to \mu\gamma$ established that μ and τ were indeed new, elementary leptons, as opposed to the excited states of composite lighter leptons. In analogy to the GIM mechanism, the absence of $\mu \to e\gamma$ also required to introduce the muon neutrino, prior to the ν_μ discovery in 1962 [6], to cancel FCNC amplitudes [7].

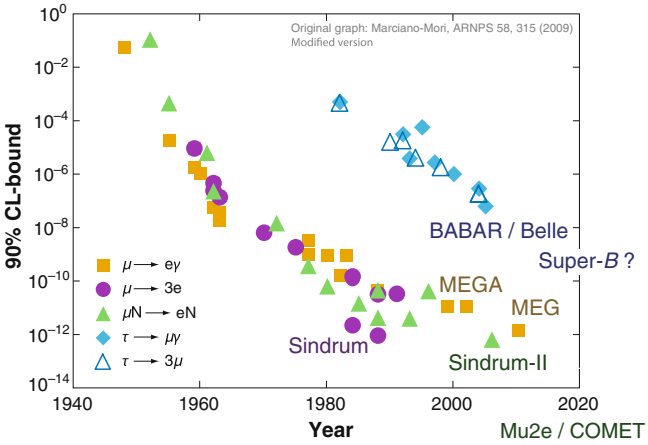

Figure 1. History of searches for selected lepton flavour-violating processes. Shown are 90% CL upper limits, and the experiments setting the best current limits and future prospectives for LFV searches in τ decays and μ–e conversion are indicated. This graph has been modified from ref. [4].

Radiative lepton decays $\ell_1 \to \ell_2\gamma$ proceed via dimension-5 left- and right-handed radiative transition amplitudes. The branching fraction can be written in the form [4]

$$\mathcal{B}(\ell_1 \to \ell_2\gamma) = \frac{3\alpha}{32\pi}\left(|A_L|^2 + |A_R|^2\right) \cdot \mathcal{B}(\ell_1 \to \ell_2\nu\bar{\nu}). \quad (1)$$

For generic new physics at mass scale Λ, one can parametrize the left- and right-handed dipole amplitudes by $A_L = A_R = 16\sqrt{2}\pi^2/G_F\Lambda^2$, where G_F is the Fermi constant and Λ is the scale of the LFV interaction. The 2002 upper limit of $\mathcal{B}(\mu \to e\gamma) < 1.2 \cdot 10^{-11}$, obtained by the MEGA experiment at the Los Alamos Meson Physics Facility [8], thus translates into the stringent bound $\Lambda > 340$ TeV [4], which is well beyond the LHC reach. Decays involving virtual photons, such as $\ell_1 \to \ell_2\bar{\ell}_2\ell_2$ and μ–e conversion, have an additional rate suppression factor α_{QED}, but also probe different physics processes.

Figure 2 depicts example graphs for R-parity conserving supersymmetric contributions to the charged LFV processes $\mu \to e\gamma$ (a) and $\mu N \to eN$ conversion (b). The predicted rates depend on the value of the slepton mass mixing parameter involved ([9,10] and references therein). LFV is also naturally present in R-parity violating models, where the strength of the effects is governed by the size of trilinear lepton number violating couplings involving sleptons and leptons (λ), and squarks, leptons and quarks (λ') in the supersymmetric superpotential [11].

2.1 *A new limit on $\mathcal{B}(\mu^+ \to e^+\gamma)$ by the MEG experiment*

The MEG experiment [12,13] uses the presently most powerful quasicontinuous muon beam produced at the PSI (Switzerland) πE5 beam line. Positive 29 MeV surface muons hit with $3 \cdot 10^7$ Hz rate a thin stopping target that is surrounded by the MEG detector. The muon decay rate measured by MEG effectively has no time structure, because the

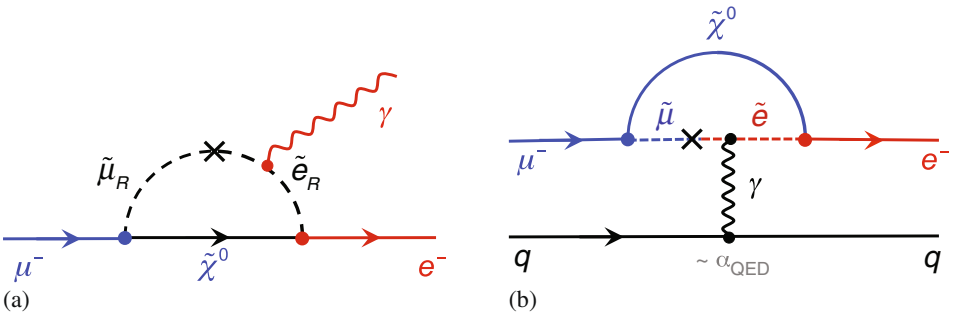

Figure 2. Possible supersymmetric contributions to the transition dipole diagrams mediating the LFV processes $\mu \to e\gamma$ (**a**) and $\mu N \to eN$ conversion (**b**).

2.2 μs muon lifetime is long compared to the 50 MHz radiofrequency structure of the proton cyclotron producing the muons. MEG consists of a positron spectrometer (drift chamber) immersed in a gradient magnetic field that sweeps the produced positrons out of the interaction region, a time-of-flight counter, and a 900 l liquid-xenon (LXe) scintillation detector outside the magnet, measuring the photon incidence, time, and energy. The solid-angle acceptance around the muon target is 10%.

The $\mu^+ \to e^+\gamma$ signal events are characterized by back-to-back, in-time monoenergetic (52.8 MeV) positron–photon pairs. Their measured energies, polar and zenith opening angles, and time difference are used to separate them from backgrounds, which are dominated by accidental coincidence of a positron from standard $\mu^+ \to e^+\nu\bar{\nu}$ decays and a photon from radiative $\mu^+ \to e^+\gamma\nu\bar{\nu}$ decays, bremsstrahlung or positron annihilation in flight. The reliance on a precise back-to-back signature invalidates the use of negative muons, which would form muonium atoms in the target that would smear out the two-body kinematics. The dominance by accidental background (that increases quadratically with the muon intensity), motivates the use of a less intense continuous beam rather than an intense pulsed beam. Ultimately, this background imposes a limitation on further progress in this channel with the current experimental techniques.

In 2010, the MEG Collaboration has released a preliminary (unpublished) result from the analysis of the 2009 data sample [14], comprising $6 \cdot 10^{13}$ μ^+ decays in the target. More than – for the null hypothesis – expected events in the signal region were found, leading to a larger than expected 90% CL limit on $\mathcal{B}(\mu^+ \to e^+\gamma)$ of $1.5 \cdot 10^{11}$, compared $6.1 \cdot 10^{12}$ expected. MEG has reanalysed the 2009 data in 2011, confirming that the excess of events is compatible with background only at the 8% level, and also included the larger 2010 dataset to a total μ^+ yield of $1.8 \cdot 10^{14}$. The 2010 data benefitted from an improved LXe waveform time resolution, but had slightly worse positron tracking resolution due to larger noise levels in the drift chamber [15]. The two-dimensional energy, angular and timing distributions of the selected events in the signal regions for the 2009 (figures 3a and b), and 2010 datasets (figures 3c and d) are shown in figure 3. The 2010 data did not reproduce the 2009 excess of signal-like events. MEG quotes the combined 90% CL upper limit [15]

$$\mathcal{B}(\mu^+ \to e^+\gamma) < 2.4 \cdot 10^{-12}\,, \tag{2}$$

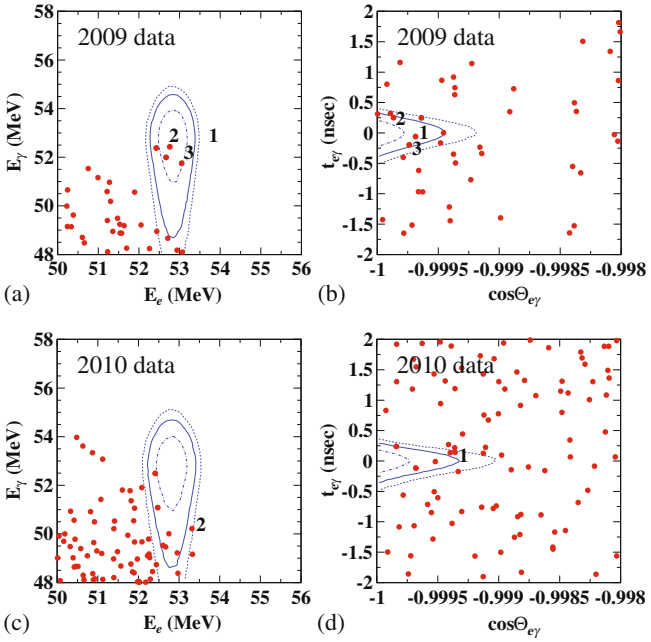

Figure 3. MEG events (solid dots) in signal regions selected in 2009 (**a** and **b**) and 2010 (**c** and **d**). Shown are the measured photon vs. positron energies and time difference vs. polar opening angle, respectively. The 1, 1.64 and 2σ signal likelihood contours are also drawn, and a few events with the highest signal likelihood are numbered for each year. The figures are taken from ref. [15] (legend modified).

compared to an expected limit of $1.6 \cdot 10^{-12}$. This result is statistically limited. Systematic uncertainties are dominated by inaccuracies in the likelihood model and normalization factors that should partly decrease with more statistics. The MEG experiment continues data taking in 2011 and 2012 to explore $\mu^+ \to e^+\gamma$ down to the design sensitivity of several 10^{-13}.

The authors of ref. [16] have explored the potential of the MEG experiment (and others) in terms of supersymmetric GUT $SO(10)$ MSUGRA models, which embed the see-saw mechanism and relate the neutrino Yukawa couplings to those of the up-quarks making them naturally large [17] so that sizable LFV effects are introduced by the renormalization group evolution. The ignorance of the Yukawa couplings between left- and right-handed neutrinos is treated using two extreme scenarios: minimal (CKM-like) and maximal (PMNS-like) mixing. Allowing MSUGRA parameter ranges of $m_0 < 5$ TeV, $-3m_0 < A_0 < 3m_0$, $\mu = \pm$, it is found that the new MEG limit excludes the maximal mixing case for large values of tan β irrespective of the $m_{1/2}$ value (see figure 6 in ref. [16]).

2.2 *Muon-to-electron conversion*

The capture of a muon in an atom and its neutrinoless conversion to an electron in the recoil field of the nucleus is denoted as μ–e conversion (see figure 2b) for a supersymmet-

ric diagram of a μ–e conversion process. In a μ–e conversion experiment, slow negatively charged muons are guided via gradient magnetic fields to hit a stopping target where they are quickly captured by an atom (within $\sim 10^{-10}$ s) and cascade down to 1S orbitals. There, the μ^- either decays (with a rate of $\sim 5 \cdot 10^5$ Hz), is weakly captured by the nucleus which undergoes β decay (exceeding the muon decay rate for heavy atoms), or converts in an LFV process to an electron via virtual photon exchange with the nucleus. The μ–e conversion gives rise to a single monoenergetic electron of 104.96 MeV for Al atoms and 95.56 MeV for Au, where the deviation from the muon mass is due to the binding energy of muonic atom and the recoil energy of nucleus. This simplicity and distinctive signature (very low background electron rate at 105 MeV, no accidentals for single-particle signature) allows extremely high rates and thus a very sensitive measurement.

The experimental observable is the conversion-to-capture ratio

$$R_{\mu e}(A, Z) = \frac{\Gamma(\mu^- + N(A, Z) \to e^- + N(A, Z))}{\Gamma(\mu^- + N(A, Z) \to \text{all } \mu^- \text{ captures})}, \tag{3}$$

where A and Z are the atomic mass and charge number, respectively. The dependence of the ratio on the atom used can be exploited to distinguish new physics models after a discovery. The denominator in eq. (3) requires the knowledge of the total number of muon captures that can be measured from standard processes. Owing to the virtual interaction of the lepton and nucleus systems, μ–e conversion is sensitive to classes of contact interaction models that do not contribute to $\mu \to e\gamma$. The conversion process might also exhibit enhanced sensitivity to supersymmetric Higgs exchange, which can be used to discriminate between models [18,19]. On the other hand, the sensitivity to generic chirality flipping dipole LFV amplitudes of new physics is reduced by factors 1/238, 1/342, 1/389 in branching ratios for Ti, Pb and Al targets, respectively [4,20,21]. This requires a more precise measurement of $R_{\mu e}(A, Z)$ than that of $\mathcal{B}(\mu \to e\gamma)$ for equal sensitivity, and hence μ^- rates of challenging 10^{11} Hz. Because no negative surface muon beams can be used, the beam will have a broader momentum spectrum and is contaminated by in-time particle backgrounds, mainly pions.

The best current limit on μ–e conversion has been obtained by the SINDRUM-II experiment at PSI in 2006 using a gold target. They found $R_{\mu e}(\text{Au}) < 7 \cdot 10^{-13}$ at 90% CL [22] (see figure 1). The extrapolated MEG sensitivity of 10^{-13} for $\mu^+ \to e^+\gamma$ requires $R_{\mu e}(A, Z) \sim 10^{-16}$. Such an accuracy is in reach of the proposed experiments Mu2e (FNAL, USA) [23] and COMET (J-PARC, Japan) [24], which have both passed important approval steps. Their goal is to achieve a sensitivity down to $(2\text{–}3) \cdot 10^{-17}$ by the year 2018, which requires to produce a total of $5 \cdot 10^{19}$ muons. The experimental approaches of Mu2e and COMET are similar, albeit with some specific differences. Mu2e uses pulsed beams of 0.6 MHz to eliminate prompt backgrounds (e.g., radiative pion capture), a pulse extinction of 10^{-10} after 0.7 μs, and exploits the late muonic atom decays ($\tau \sim 1$ μs) for the conversion measurement. A magnetic bottle traps pions produced by proton bombardment in a target, which decay into accepted muons. Gradient magnetic fields guide the muons through an S-shaped beam line from the production to the stopping target to increase the muon acceptance and momentum selection, and to evacuate loopers. Collimators reduce backgrounds from particles other than muons. For detection, the atoms pass through a tracking detector and are stopped in a calorimeter. The decay electrons describe a helix trajectory in the gradient field of a solenoid where their momentum is

precisely measured. The expected event yields for $R_{\mu-e} = 10^{-16}$ are ∼4 signal and 0.2 background events (dominated by radiative pion capture and decay-in-orbit muons). The multiple ring structure at FNAL allows to run Mu2e without interfering with the NOvA operation. COMET uses a C-shaped solenoid for improved muon momentum selection prior to hitting the stopping target, and in addition a C-shaped detector section (before the tracker) to eliminate low-energetic decay-in-orbit muons. Fascinating long-term upgrade projects, using muon storage rings that can improve the μ–e conversion sensitivity by two orders of magnitude, would be offered by an experiment at the Project-X proton accelerator complex at FNAL [25] and by the PRISM/PRIME [26] at J-PARC (site not fixed).

2.3 *Lepton flavour violation in τ decays*

The complexity of τ production in accelerators renders the search for LFV in τ decays more challenging than for muons, which are conveniently produced from pion decays. The best current sensitivity for $\tau \to \ell\gamma$ decays (charge averaged), based on a sample of almost 1 billion single τ decays, is obtained by the BABAR experiment setting 90% CL upper limits of $3.3 \cdot 10^{-8}$ (for $\ell = e$) and $4.4 \cdot 10^{-8}$ (μ) [27]. The most stringent upper limit of $1.8 \cdot 10^{-8}$ for LFV in τ decays has been obtained by the Belle experiment in the mode $\tau \to \mu\rho^0$ [28] (see ref. [5] for a full compilation of the results). Super-B projects in

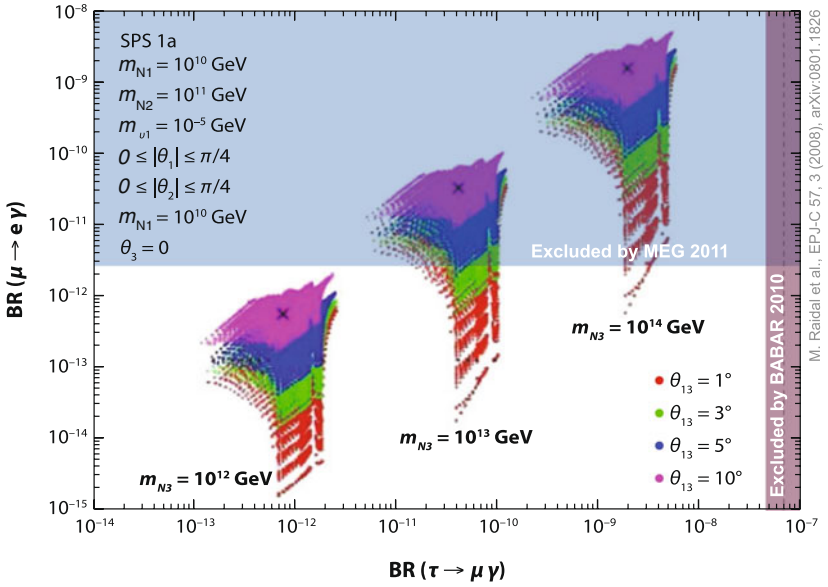

Figure 4. Correlation between $\mu \to e\gamma$ and $\tau \to \mu\gamma$ branching fractions for various values of the third-generation right-handed neutrino mass, m_{N3}, and the PMNS mixing angle, θ_{13}, in a minimal supersymmetric see-saw model and assuming the MSUGRA point SPS1a [10]. The shaded areas indicate the experimentally excluded regions (figure taken from ref. [10] (modified)).

Italy [29] and Japan [30], with anticipated integrated luminosities reaching up to 50 ab^{-1}, can improve the $\tau \to \ell\gamma$ sensitivity to a few 10^{-9} [31].

What is the expected sensitivity to new physics of $\tau \to \ell\gamma$ compared to $\mu \to e\gamma$? This question can be addressed in specific new physics models by comparing the predicted branching fractions as a function of the model parameters. Such a study has been performed in ref. [10], the results of which, for a minimal supersymmetric see-saw model and assuming the MSUGRA point SPS1a, is shown in figure 4. The various regions correspond to different assumptions for the heavy neutrino mass and the θ_{13} mixing angle. If the recent T2K result [32] on $\nu_\mu \to \nu_e$ appearance is confirmed (the significance of the current ν_e appearance excess is evaluated to be 2.5σ), θ_{13} should be larger than 5°, hence effectively excluding the $m_{\mathrm{N3}} = 10^{14}$ GeV case. A large mixing angle leads to similar contributions to both LFV decays which renders the τ channel non-competitive. Similar results are found in ref. [33], where also a study using $SU(5)$ without right-handed neutrinos is performed exhibiting larger differences between the $\tau \to \ell\gamma$ and $\mu \to e\gamma$ branching fractions, although the predicted effects are smaller in general than for supersymmetric GUT see-saw models.

3. Electric dipole moments

Elementary particles are predicted to be non-spherical, distorted by an electric dipole moment (EDM). However, as for charged LFV, EDMs are predicted to be undetectably tiny in the SM. Thus, any hint for a non-zero EDM would be a clean probe for physics beyond the SM, and indeed many SM extensions predict EDMs that are detectable by current experiments.

Electric dipole moments are CP-violating. The Hamiltonian of a system with magnetic moment, μ, and EDM, d, immersed in magnetic and electric fields, $\vec{B}$ and $\vec{E}$, is given by $H = -\mu\vec{B}\cdot\hat{S} - \mathrm{d}\vec{E}\cdot\hat{S}$ (describing a magnetic and electric Zeeman effect), where $\hat{S}$ is the unit spin vector. Applying P and T transformations on H, we find that the product $\vec{B}\cdot\hat{S}$ transforms even under both P and T, while $\vec{E}\cdot\hat{S}$ transforms odd under these so that, assuming CPT invariance, a non-zero EDM is CP non-conserving.

All experiments searching for EDMs follow the same basic principle. A particle with spin-1/2 immersed in magnetic and electric fields sees its spin vector precessing with Larmor frequency $\omega_{\uparrow\uparrow} = 2(\mu B + \mathrm{d}E)/\hbar$, where the arrows indicate that both B and E fields have parallel orientation. Given the strong existing limits on d, a small value of $d \sim 10^{-26}$ e cm in an electric field of 10 kV/cm induces a tiny precession frequency of 0.1 μHz. This frequency corresponds to a magnetic field strength of 20 pG for a neutron [34]. Given that already the magnetic field of the Earth amounts to 0.2–0.7 G, it is obviously impractical to measure the E-induced offset and thus d directly. The effect of B (if time-independent) can be cancelled by flipping the sign of the E field and thus determining the frequency difference $\Delta\omega = \omega_{\uparrow\uparrow} - \omega_{\uparrow\downarrow} = 4\mathrm{d}E/\hbar$. The sensitivity of the experiment thus depends on the control of the B field variations between two E flips, and on the E field strength. As we shall see later, the effective E field seen by the dipole can be strongly amplified in paramagnetic atoms and molecules.

Figure 5 depicts the hierarchy of scales between CP-odd sources and generic classes of observable EDMs [35]. On top, at TeV scale or beyond, the unknown source of CP

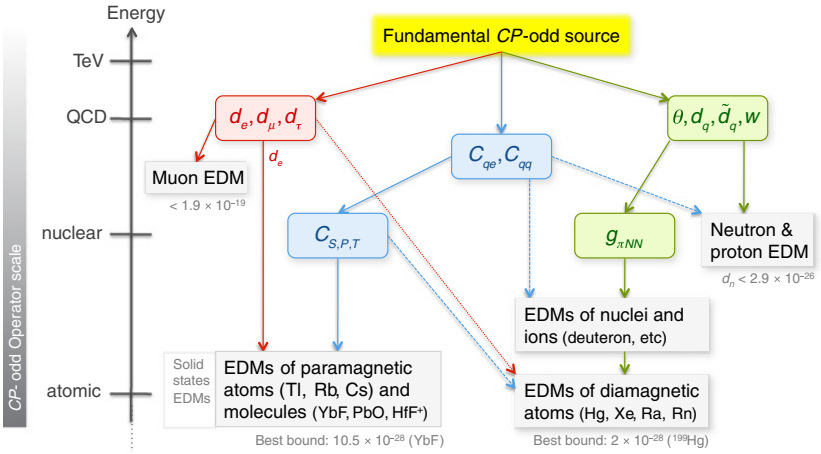

Figure 5. Hierarchy of scales between CP-odd sources and generic classes of observable EDMs (figure inspired by refs [10,35,36]).

violation gives rise to lepton, light quark and colour EDMs at QCD scale, or a QCD θ term. The latter term is the only dimension-four operator and is thus not scale-suppressed. This and the empirical smallness of θ is what is known as the strong CP problem. The EDMs formally belong to dimension-five operators, while most new physics models place them at dimension six (generating chirality flips) so that the EDMs are quadratically suppressed by the new physics scale, which makes them naturally small for high-scale new physics. The w term in figure 5 stands for a genuine dimension-six three-gluon operator. The C_{ij} terms are the coefficients of four-fermion operators, which are of dimension six or, in models with chirality flips, of dimension eight. These CP-odd parameters are either directly observable, as is the case of the lepton EDMs, or induce CP-odd operators at the nuclear scale. The most upfront observables at this scale are the neutron and proton EDMs, which directly arise from CP-odd sources at the quark-gluon level. At the atomic scale, when dealing with nuclei, ions, and atoms, CP-odd pion–nucleon interactions also must be considered (denoted $g_{\pi\mathrm{NN}}$ in figure 5). When EDMs are studied at the atomic scale, one distinguishes CP-odd effects induced in paramagnetic and diamagnetic atoms or molecules. Paramagnetic atoms (named for their unpaired electrons, e.g., thallium) and molecules (e.g., ytterbium–fluorine), are mainly sensitive to the electron EDM and CP-odd electron–nucleon couplings (denoted $C_{\mathrm{S,P,T}}$ in figure 5). Diamagnetic atoms (e.g. mercury) receive the same CP-odd contributions as paramagnetic atoms, but they are strongly suppressed due to smaller Schiff shielding violation, so that contributions from pion–nucleon scattering must also be considered.

3.1 *Neutron and proton EDMs*

A chronological overview of the neutron EDM measurements is shown in figure 6. The development of ultracold neutron (UCN) facilities provided a large sensitivity boost in

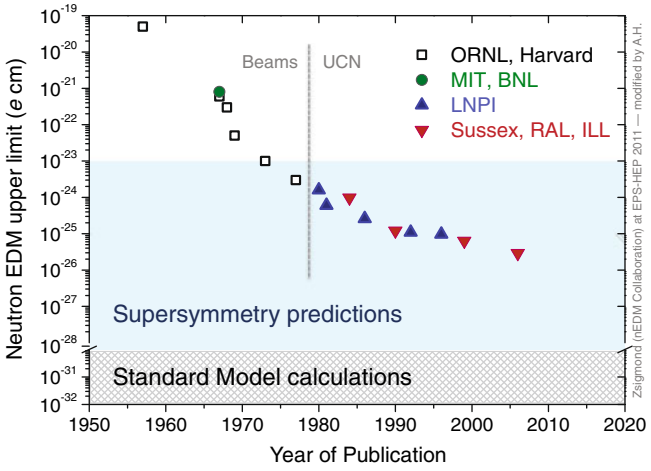

Figure 6. History of neutron EDM measurements. The vertical line indicates the switch to ultracold neutron facilities. Also shown are ball-park ranges of generic supersymmetry and SM predictions. For completeness one should also add solid-state EDM effects to the atomic scale (figure taken from ref. [37] (modified)).

this very active research field. Techniques such as the use of *in situ* diamagnetic comagnetometers allowed to reduce systematic uncertainties due to magnetic field fluctuations. The currently best limit of $|d_n| < 2.9 \cdot 10^{-26}$ e cm at 90% CL has been obtained by the Sussex-RAL-ILL experiment operating at the ILL-Grenoble, France [38]. We can use it to illustrate the strong CP problem, $|\theta| \sim |d_n| \cdot 2 \cdot 10^{16} < 5 \cdot 10^{-10}$, and the supersymmetry problem, $|d_n| \sim 10^{-23}\, e\,\text{cm} \cdot (300\ \text{GeV}/M_{\text{SUSY}})^2 \cdot \sin\phi_{\text{SUSY}}$, where M_{SUSY} and ϕ_{SUSY} are the generic supersymmetry mass scale and CP-odd phase value, respectively (see, e.g., [35]). Both parameters are subject to large suppression.

Further improvement in the neutron EDM sensitivity requires to increase the UCN density, which can, for example, be achieved by using superfluid ^{4}He used to moderate and store UCNs. Future experiments [36] aim at sensitivities of (in units of $10^{-26} e$ cm) 0.5 and 0.05 for the nEDM (by 2013) and n2EDM experiment at PSI (2016), respectively, 1 for PNPI at ILL (2012), 0.3 for CryoEDM at ILL (2016), 0.03 for nEDM at SNS-ORNL (2020), 1 for nEDM at RCNP (2014), 0.1, and 0.01 for nEDM at TRIUMF (2017 and $>$2020).

A fascinating perspective for the measurements of proton and/or light ion EDMs offers new proposals at BNL, USA [39] and Jülich, Germany [39], with an anticipated sensitivity of 10^{-29} e cm [40]. The proposed experiments exploit a similar magic gamma trick as used for the measurement of the muon anomalous magnetic moment in a homogeneous magnetic field, but here applied to a radial electric field that keeps the particles on orbit. A magic proton moment of 0.7 GeV leads to aligned proton spin and momentum vector precession ($\omega_a = 0$), thus allowing a precise EDM measurement by monitoring any vertical spin precession vs. time. Assuming that the sensitivity to new physics is the same for protons and neutrons, these certainly are must-explore experiments.

3.2 *Electron EDM*

For many years, the electron EDM was dominated by the famous Berkeley measurement using thallium atoms that achieved in 2002 a 90% CL upper limit of $|d_e| < 1.6 \cdot 10^{-27}$ e cm [41]. Again, this limit cuts into the bulk predictions of, e.g., supersymmetry, left–right symmetric and multi-Higgs models, while the SM prediction lies even several orders of magnitude below that for the neutron EDM. I shall describe here a recent measurement performed at the IC-London, UK, using YbF molecules [42].

Paramagnetic atoms and molecules respond to a screening theorem by Schiff [43] that implies a vanishing net EDM for a system built entirely from point-like, non-relativistic constituents that interact only electrostatically. Schiff's theorem is broken by magnetic and relativistic interactions, and by finite size effects, i.e., a misalignment between the distribution of charge and EDM in the atom or molecule. Schiff violation is stronger for heavy atoms (growing as Z^3) and even stronger for polarizable molecules. It leads to an enhancement of the applied electric field, with factors of roughly -585 for the spherical thallium and 1.4 million for the dipolar YbF. The YbF factor is given for an external E field of 10 kV/cm, not rising linearly with the strength of the field due to saturation effects (see ref. [44] and references therein). Other advantages of YbF over Tl are smaller systematic uncertainties, in particular those to motional magnetic fields. A shortcoming, however, is the much smaller production rate of YbF.

The ICL YbF electron EDM experiment looks for a spin interferometer phase shift of the $F = 0, 1$ YbF hyperfine levels when the electric field is reversed. The principle of the table-top apparatus is depicted in figure 7 (taken from ref. [42]). Laser-ablated YbF molecules populating both hyperfine levels are depleted from $F = 1$ states via laser pumping using the 552 nm optical transmission line of YbF. The remaining molecules in the $F = 0$ ground state enter a pair of electric field plates (magnetically shielded). A tuned 170 MHz radiofrequency (RF) pulse transfers the molecules into the $F = 1$ hyperfine level, where they form a coherent $(|F = 1, m_F = 1\rangle + |1, -1\rangle)/\sqrt{2}$ state. While travelling some time T, the magnetic and electric (if non-zero EDM) fields induce a phase shift [42] $(e^{i\phi}|1, 1\rangle + e^{-i\phi}|1, -1\rangle)/\sqrt{2}$, where $\phi = (\mu_B B - d_e E_{\text{eff}}) \cdot T/\hbar$. Another RF pulse projects the phase-shifted molecules back to $F = 0$ with state function $(e^{i\phi} + e^{-i\phi})|0, 0\rangle/2$. A fluorescence pump detector counts the $F = 0$ population that has a

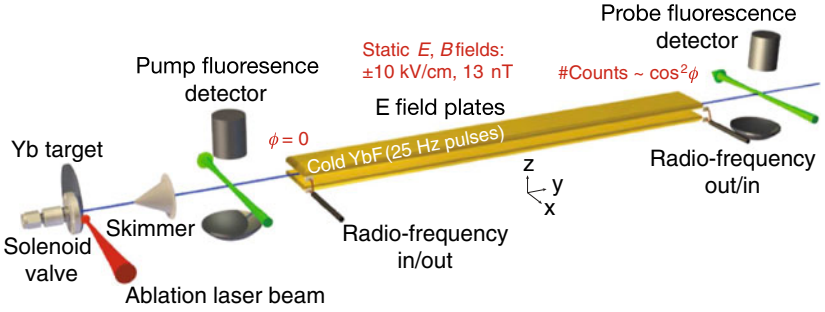

Figure 7. Sketch of the ICL YbF electron EDM experiment [42] (modified). Pulsed YbF molecules travel from the left to the right in between the electric field plates.

rate proportional to $\cos^2\phi$. One can scan the counting rate and thus ϕ by modulating the external magnetic field, and generate a tiny observable phase shift $\Delta\phi = 2d_e E_{\rm eff} T/\hbar$ by reversing the electric field. In practice, the B and E fields as well as several other parameters of the apparatus are switched in a random sequence between each beam pulse to track and minimize systematic correlations.

A total of 25 million YbF beam pulses, distributed throughout 6000 data blocks taken in 2010, give eight statistically independent measurements corresponding to manual reversal states of the apparatus. Combined they yield $d_e = (2.4 \pm 5.7_{\rm stat} \pm 1.5_{\rm syst}) \cdot 10^{-28}\ e$ cm, and a 90% CL upper limit of $|d_e| < 10.5 \cdot 10^{-28}\ e$ cm. The systematic error is currently dominated by the uncertainty in the uniformity of E between sign flips [42].

This pioneering measurement has great potential in spite of, yet, relatively little improvement over the 2002 thallium result. The present result is statistically limited, and systematic errors are expected to be reducible to a level of $<10^{-29}\ e$ cm. The ICL group aims at a factor of 10 sensitivity improvement within a few years, with the final goal of reaching a factor of 100 improvement. Several other EDM experiments, based on electron spin precession in atoms, molecules, molecular ions or solids are in progress.

4. Tau-lepton physics

The 20th anniversary of the Tau Workshop series which started at LAL-Orsay in 1990 was celebrated last year. During that period, there was magnificent progress in τ-lepton physics through the LEP, CLEO, B-factory, BES, VEPP-2M, and neutrino experiments. Early Tau Workshops concentrated on the consolidation of the τ as a standard lepton without invisible decays and with universal couplings. Increased data samples as well as better understanding and methods allowed the experiments to study electroweak and QCD physics with τ leptons leading to precision measurements of fundamental SM parameters such as $\sin^2\theta_{\rm W}$, $\alpha_{\rm s}$, and $|V_{us}|$.

Each of the four LEP experiments (1989–2000, CERN, Switzerland) collected a data sample of roughly 165,000 $Z \to \tau\tau$ events, CLEO (1979–2008 at CESR, Cornell, USA) already disposed of about 3.6 million τ pairs, albeit with less efficient and pure selection. The B-factory experiments BABAR at SLAC, USA and Belle at KEK-B, Japan accumulated breathtaking 500 million and 900 million τ pairs, respectively. Consequently, these experiments concentrate on rare modes and searches for new physics: lepton flavour violation in tau decays, charged weak current universality tests, rare branching fractions, second class currents (isospin violation), and CP violation. Phenomenological work on the determination of $\alpha_{\rm s}$ and $|V_{us}|$ from τ branching fractions and spectral functions are also actively pursued.

4.1 *Tau branching fractions and tests of universality*

The most recent summary of the τ branching fractions is available from the Heavy Flavour Averaging Group (HFAG) [5] (see τ section). The dominant leptonic and hadronic τ branching fractions have been measured to great precision at LEP while running at Z resonance. The ALEPH experiment in addition performed a global analysis of all τ hadronic modes imposing unitarity [45]. The B-factory experiments also contributed with many

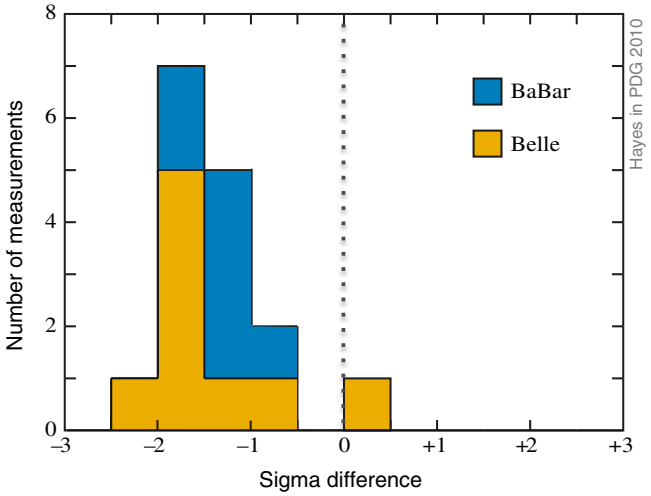

Figure 8. Pull difference between the 16 *B*-factory measurements of τ branching fractions and their non-*B*-factory measurements. Belle and BABAR have each published eight measurements (figure from ref. [46] (colours modified)).

new measurements, in particular improving the modes with kaons owing to their superior particle identification capabilities. The PDG group [46] noticed a puzzling tendency when comparing the total of 16 *B*-factory measurements (upper limits and exotic searches not included) with their counterparts from LEP: all but one *B*-factory results lie systematically below those from LEP (figure 8). This is a feature that requires further scrutiny.

The measurements of the branching fractions involving leptons allow to test the three-generation universality of the charged weak current. The HFAG finds for the weak coupling ratio $|g_\mu/g_\varepsilon|$ obtained from the ratio of the $\tau \to \mu\bar{\nu}\nu$ to $\tau \to e\bar{\nu}\nu$ world average branching fractions (corrected for mass-dependent effects) 1.0018 ± 0.0014 [5], which is a factor of 7 more precise than the measurement of the corresponding on-shell W leptonic branching fraction ratio [46]. It is of similar precision as the universality tests performed in neutral current reactions at LEP, giving 0.28% from a comparison of the $Z \to \ell\ell$ branching fractions, and 0.13% from comparing the effective weak axial coupling $g_{A,e/\hat{\mathrm{l}}\mathrm{ij}}$ [47]. Universality of the ratios $|g_\tau/g_\varepsilon|$ and $|g_\tau/g_\mu|$ can be tested by comparing the measured τ leptonic branching fractions with the predicted ones using the τ and muon lifetimes and correcting for mass and radiative effects. The HFAG computes the world average ratios 1.0027 ± 0.0021 and 1.0008 ± 0.0021, respectively. Finally, the ratio $|g_\tau/g_\mu|$ can also be precisely determined with the ratio of $\tau \to h\nu$ to $h \to \mu\nu$ ($h = \pi, K$) branching fractions, corrected for mass and radiative effects, which gives 0.9949 ± 0.0029. None of these tests reveals a significant deviation from universality.

4.2 *Second class currents*

In τ decays the charged weak current is classified according to its G-parity, where $J^{\mathrm{PG}} = 0^{--}, 1^{+-}$ currents (π, a_1, ...) produce an odd number of pions in the final

state, and $J^{\rm PG} = 1^{-+}$ currents (ρ, ...) produce an even number of pions. These are denoted first class currents. Second class currents [48] (SCC) have opposite spin-parity $J^{\rm PG} = 0^{+-}, 0^{-+}, 1^{++}$, or 1^{--}. They violate isospin symmetry and thus vanish in the strict isospin limit. Their branching fractions are expected to be proportional to the u, d quark mass difference-squared. Examples for SCC are the $\tau \to \eta\pi\nu$ and $\tau \to\to \omega\pi\nu$ decays, which may be dominantly mediated by the $a_0(980)$ and $b_1(1235)$ resonances, respectively. Estimates predict $\mathcal{B}(\tau \to \eta\pi\nu) = (1.3 \pm 0.2) \cdot 10^{-5}$ (see refs [49,50] and references therein). No SCC mode has been observed to date. The best current experimental limit, $9.9 \cdot 10^{-5}$ at 90% CL, has been obtained by BABAR using the full available statistics [51]. Since this search is not free of background, a much larger data sample is required to be able to discover this mode if the branching fraction is as expected.

4.3 *CP violation in τ decays*

CP violation in τ decays with strangeness occurs in the SM via mixing-induced CP violation in the neutral kaon system. The asymmetry

$$A_{\rm Q} = \frac{\Gamma(\tau^+ \to \pi^+ K^0_{\rm S} \bar{\nu}_\tau) - \Gamma(\tau^- \to \pi^- K^0_{\rm S} \bar{\nu}_\tau)}{\Gamma(\tau^+ \to \pi^+ K^0_{\rm S} \bar{\nu}_\tau) + \Gamma(\tau^- \to \pi^- K^0_{\rm S} \bar{\nu}_\tau)}\,, \tag{4}$$

is predicted to be $A_{\rm Q}^{\rm SM} \simeq 2{\rm Re}(\varepsilon_{\rm K}) = (0.33 \pm 0.01)\%$ [52]. Reference [53] (appeared after the conference) points out that this prediction for the $K^0_{\rm S}$-only terms contains a sign mistake and that only when taking into account $K^0_{\rm S}$–$K^0_{\rm L}$ interference, the positive sign is approximately recovered. Deviations from $A_{\rm Q}^{\rm SM}$ should have new physics origin as is possible, e.g., in multi-Higgs models [54]. Results consistent with the SM were previously found in $D^\pm \to K^0_{\rm S}\pi^\pm$ [55] and in an angular analysis of $\tau^\pm \to \pi^\pm K^0_{\rm S}\nu$ [56].

For the conference, BABAR released a new result for $A_{\rm Q}$ [57] based on the full available dataset (476 fb^{-1}). The analysis uses electron- and muon-tagged events (recoil side). The raw asymmetry is corrected for different nuclear interaction cross-sections and for feed-through from $K^0_{\rm S}K^\pm(\geq\pi^0)$ and $K^0\bar{K}^0\pi^\pm$) decays, where $A_{\rm Q}^{\rm SM}$ is assumed for the latter correction. BABAR finds $A_{\rm Q} = (-0.45 \pm 0.24 \pm 0.11)\%$, which deviates by $\sim 3\sigma$ from $A_{\rm Q}^{\rm SM}$. However, as argued in ref. [53], the precise prediction of $A_{\rm Q}$ as measured by BABAR must account for the decay time interval over which it is measured, which depends on the applied experimental conditions and analysis requirements.

4.4 *Tau hadronic spectral functions and QCD*

QCD studies using the τ hadronic width and spectral moments computed from the τ hadronic spectral functions have traditionally been the most active field of phenomenological studies involving τ physics (see, e.g., ref. [58] for a review). In particular, the measurements of the complete vector and axial-vector tau hadronic spectral functions by ALEPH [45,59,60] and OPAL [61] triggered widespread interest. Most prominently, τ decays allow an accurate determination of $\alpha_{\rm s}$ from the comparison of the non-strange τ hadronic width, $R_{\tau,{\rm V+A}} = 3.4771 \pm 0.0084$ [5], precisely obtained using unitarity and universality from the measurements of the leptonic branching fraction and the τ lifetime,

and subtracting the strangeness contribution, with the SM prediction from essentially perturbative QCD. Small non-perturbative contributions are fitted from data using the spectral moments. Quark-hadron duality violations are usually assumed to be negligible due to the suppression of the spectral moments at the τ mass (see the critical discussion in ref. [62]). The perturbative QCD prediction of $R_{\tau,\mathrm{V+A}}$ benefits, as the electroweak fit of the Z hadronic width, from an NNNLO calculation of the massless perturbative Adler function [63]. Unfortunately, an ambiguity in the perturbative treatment does not currently allow one to fully exploit the available precision [64–67].

From the combined fit of α_s and the non-perturbative terms to $R_{\tau,\mathrm{V+A}}$ and several spectral moments, and after renormalization group evolution from the τ to the Z mass, one finds

$$\alpha_\mathrm{s}(M_\mathrm{Z}) = 0.1200 \pm 0.0005_\mathrm{exp} \pm 0.0008_\mathrm{theo} \pm 0.0013_\mathrm{CIPT/FOPT} \pm 0.0005_\mathrm{evol}\,, \tag{5}$$

where the first error is experimental, the second theoretical, the third accounts for half of the difference between the two perturbative treatments (denoted as contour-improved and fixed-order perturbation theory, of which the average result is used as central value for $\alpha_\mathrm{s}(M_\mathrm{Z})$), and the last error accounts for the evolution uncertainty (four-loop evolution [68] with three-loop quark-flavour matching [69–71]). The non-perturbative contributions in

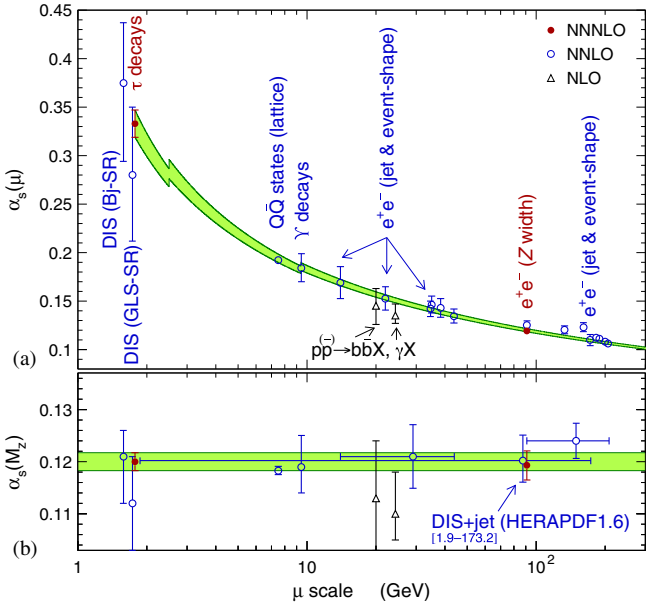

Figure 9. (**a**) Evolution of $\alpha_\mathrm{s}(m_\tau^2)$ to higher scales μ using the four-loop RGE and the three-loop matching conditions applied at twice the heavy quark-pair thresholds (hence the discontinuities). The evolution is compared with independent measurements (taken from the compilation [73]), covering μ scales that vary more than two orders magnitude. (**b**) The corresponding α_s values evolved to M_Z. The shaded band displays the τ decay result within errors (figure courtesy: Z Zhang).

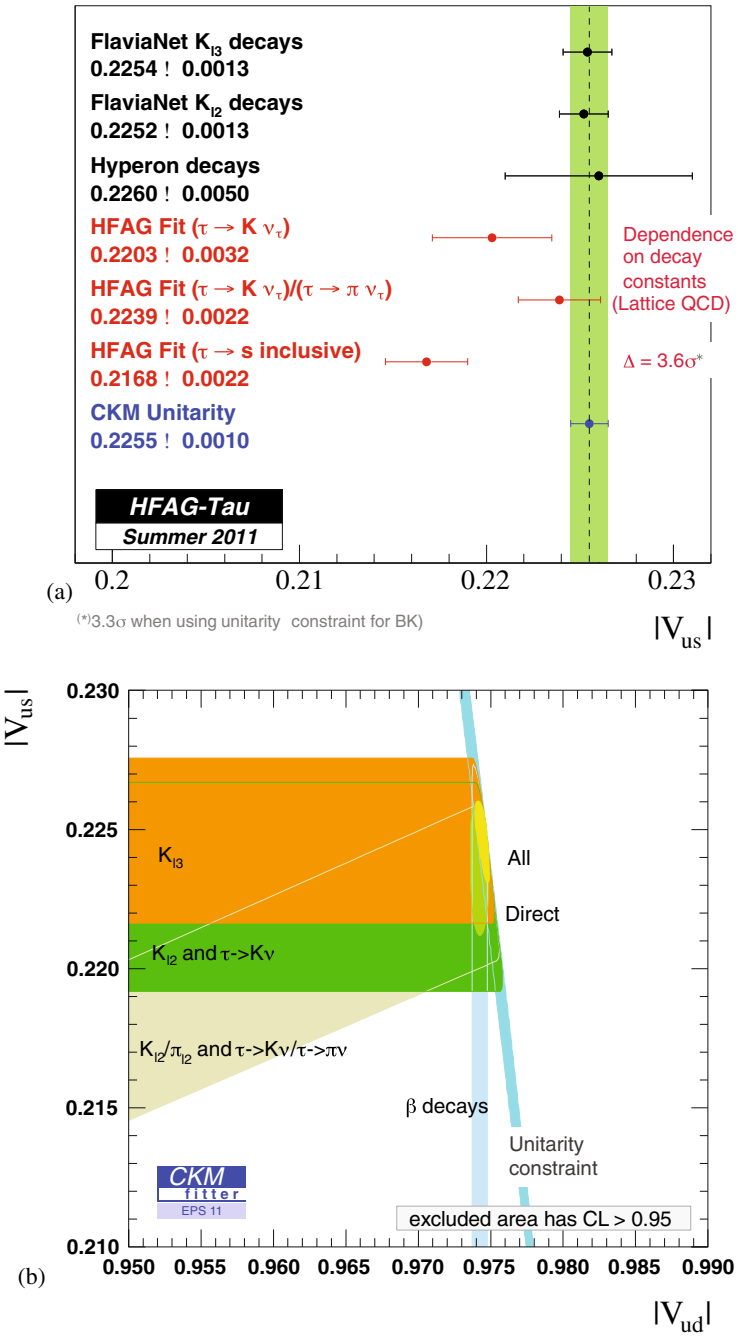

Figure 10. (**a**) Determination of $|V_{us}|$ [5]. The results from τ decays are printed in red. (**b**) $|V_{us}|$ vs. $|V_{ud}|$. Shown are recent experimental determinations of these quantities and the constraint from unitarity in the first row of the CKM matrix [76].

eq. (5) are taken from ref. [64]. Equation (5) is in excellent agreement with the NNNLO result from the electroweak fit to (mainly) the Z hadronic width $\alpha_s(M_Z) = 0.1193 \pm 0.0028$ [72], providing a precise test of the asymptotic freedom property of QCD. The evolution path of $\alpha_s(m_\tau^2)$ is shown in figure 9a. The evolution is compared in this plot with other α_s determinations compiled in ref. [73].

4.5 *Determination of* $|V_{us}|$

The amount of net strangeness production in τ decays is directly proportional to the CKM element $|V_{us}|^2$. Accurate extractions of this element have been performed using three different methods: (i) comparing the measured branching fraction of the $\tau^- \to K^-\nu$ decay with its SM prediction, which depends on the kaon decay constant taken from lattice QCD and on radiative corrections, (ii) comparing the measured ratio of the $\tau^- \to K^-\nu$ and $\tau^- \to \pi^-\nu$ branching fractions to the SM prediction, and (iii) comparing the inclusive τ strange hadronic width with its SM prediction. The latter two methods also depend on $|V_{ud}|^2$.

The results for $|V_{us}|$ obtained from these methods are shown figure 10a, and are compared to other evaluations and to the CKM fit result assuming unitarity. The figure is taken from ref. [5]. The agreement between the τ inclusive result and the CKM fit is marginal. The inclusive method uses the observable $|V_{us}|^2 = R_{\tau,S=1}/(R_{\tau,S=0}/|V_{ud}|^2 - \delta R_\tau^{SM}(\alpha_s, m_s))$, where the SM prediction of the mass-dependent term, $\delta R_\tau^{SM}(\alpha_s, m_s)$, exhibits slow convergence in the perturbative series [74,75], which leads to hard-to-quantify theoretical uncertainties. The inclusive method may also suffer from potentially unmeasured modes, which are not included in the systematic uncertainties. Finally, the trend to smaller branching fractions from the B-factory experiments has a non-negligible impact. Without the B-factory data, $|V_{us}|$ from the inclusive determination will increase to $\sim$0.2213. A precise measurement of the full strange spectral function by the B-factory experiments should help one to test the inclusive method.

Figure 10b shows the experimental results on V_{us} vs. V_{ud} compared to the CKM fit constraint [76]. Good agreement with unitarity of the first row is observed.

5. Anomalous magnetic moment of the muon

For elementary leptons, ℓ, the Dirac equation predicts a magnetic moment, $\vec{M} = (g_\ell e/2m_\ell) \cdot \vec{S}$, with gyromagnetic ratio $g_\ell = 2$ [77]. Quantum fluctuations lead to a small calculable deviation from $g_\ell = 2$, parametrized by the anomalous magnetic moment $a_\ell \equiv (g_\ell - 2)/2$. That quantity can be accurately measured and, within the SM, precisely predicted. Hence, comparison of experiment and theory tests the SM at its quantum loop level. A deviation in a_ℓ^{exp} from the SM expectation would signal effects of new physics, with current sensitivity reaching up to mass scales of $\mathcal{O}$(TeV) for $\ell = \mu$ [78,79]. Considering the expected quadratic dependence of new physics contributions on the lepton mass [78], and the current experimental uncertainties on a_ℓ^{exp}, the muon $g-2$ is roughly 50 times more sensitive to new physics than the electron one [79a], while the tau $g-2$ has not yet been measured to significant precision. For recent and very thorough muon $g-2$ reviews, see refs [85,86].

5.1 *Experimental result*

The E821 experiment at Brookhaven National Lab (BNL), USA, studied the precession of μ^+ and μ^- in a uniform external magnetic field perpendicular to the muon spin and orbit plane as they circulated in a cyclotron. At a magic muon momentum of 3.09 GeV (or magic $\gamma = 29.3$), and negligible μ EDM, the observed difference between spin precession frequency and cyclotron frequency, ω_a is independent of the focussing electric field and is given by $\omega_a = a_\mu Be/m_\mu c$. Following a doubly blinded analysis strategy, E821 found the charge averaged result [87–89] as

$$a_\mu^{\text{exp}} = (11\,659\,208.9 \pm 5.4 \pm 3.3) \cdot 10^{-10}\,, \tag{6}$$

where the first error is statistical and the second is systematic. This result represents about a factor of 14 improvement over the classic CERN experiments of the 1970s [90].

5.2 *Standard Model prediction*

The SM prediction for a_μ^{SM} is conveniently divided into three parts (see figure 11 for representative Feynman diagrams)

$$a_\mu^{\text{SM}} = a_\mu^{\text{QED}} + a_\mu^{\text{EW}} + a_\mu^{\text{had}}\,. \tag{7}$$

The QED part includes all photonic and leptonic (e, μ, τ) loops starting with the classic $\alpha/2\pi$ Schwinger contribution [91]. It has been computed through four loops and estimated at the 5-loop level [92–97]. Employing $\alpha^{-1} = 137.035999084 \pm 51$, determined [80,92–98] from the electron a_e measurement, leads to $a_\mu^{\text{QED}} = (116\,584\,718.09 \pm 0.15) \cdot 10^{-11}$, where the error results from uncertainties in the coefficients of the perturbative series and in α. Loop contributions involving heavy $W^\pm$, Z, or Higgs particles are collectively labelled as a_μ^{EW}. They are suppressed by at least a factor of $(\alpha/\pi)\cdot(m_\mu/m_{\text{W}})^2 \simeq 4 \cdot 10^{-9}$. At 1-loop order, one finds $a_\mu^{\text{EW}}[\text{1-loop}] = 194.8 \cdot 10^{-11}$ [99]. Two-loop corrections are found to be relatively large and negative, $a_\mu^{\text{EW}}[\text{2-loop}] = (-40.7 \pm 1.0 \pm 1.8) \cdot 10^{-11}$ [100–106], where the errors stem from quark triangle

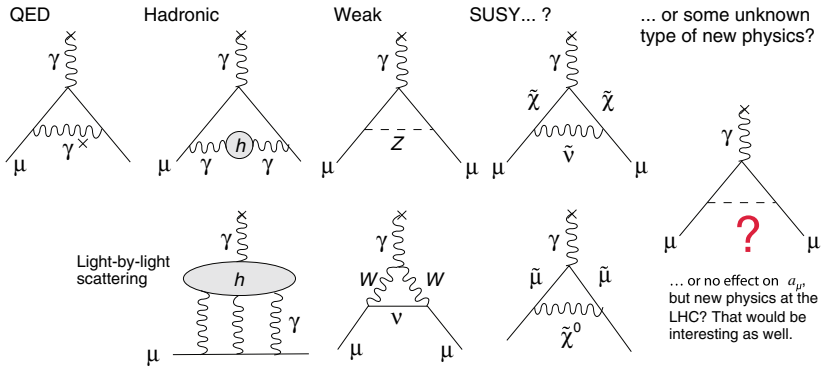

Figure 11. Feynman graphs contributing to a_μ^{SM} and possible new physics processes.

loops and the assumed Higgs mass range between 100 and 500 GeV. The 3-loop leading logarithms are negligible [100,107], $\mathcal{O}(10^{-12})$, implying the total weak contribution $a_\mu^{\mathrm{EW}} = (154 \pm 1 \pm 2) \cdot 10^{-11}$.

5.3 *Hadronic contribution*

Hadronic loop contributions to a_μ^{SM} give rise to its main theoretical uncertainties. At present, those effects are not calculable from first principles, but such an approach, at least partially, may become possible as lattice QCD matures (see [108] for a lattice calculation using two-flavour QCD which results, however, in an underestimate of $a_\mu^{\mathrm{SM},n_f=2}$). Instead, one currently relies on a dispersion relation approach to evaluate the lowest-order hadronic vacuum polarization contribution, $a_\mu^{\mathrm{had,LO}}$, from the corresponding cross-section measurements and predictions [109,110]

$$a_\mu^{\mathrm{had,LO}} = \frac{1}{3}\left(\frac{\alpha}{\pi}\right)^2 \int_{m_\pi^2}^{\infty} \mathrm{d}s \, \frac{K(s)}{s} R^{(0)}(s)\,, \tag{8}$$

where $R^{(0)}(s)$ denotes the ratio of the bare cross-section for e^+e^- annihilation into hadrons to the point-like muon-pair cross-section at the centre-of-mass energy $\sqrt{s}$. The function $K(s) \sim 1/s$ gives a strong weight to the low-energy part of the integral [111], such that $a_\mu^{\mathrm{had,LO}}$ is dominated by the $\rho^0(770) \to \pi^+\pi^-$ resonance.

There has been a huge, 20-year long effort by experimentalists and theorists to reduce the error on $a_\mu^{\mathrm{had,LO}}$. It featured improved e^+e^- cross-section data from the Novosibirsk, Russia accelerator facilities, more use of perturbative QCD to replace inaccurate data points, the development of the radiative return technique which allows to exploit cross-section data from the high-luminosity Φ and B factories, and the use of precise τ hadronic spectral functions by applying isospin symmetry. The computation of the integral (8) proceeds in different steps. Exclusive cross-section measurements are summed up to obtain $R^{(0)}(s)$ for $\sqrt{s} \leq 1.8$ GeV. Unmeasured modes are estimated from measured ones using isospin relations. Perturbative QCD can be used to predict $R^{(0)}(s)$ away from the quark thresholds in the quark–antiquark continuum. Comparisons of the QCD predictions with inclusive data, where available, exhibit good agreement with theory. The so-called global quark-hadron duality approximation is helpful here, which uses the fact that essentially perturbative QCD can be used to predict integrals over hadronic spectral functions if a large enough spectrum is integrated over and if the end-point of the integral is not too far from the continuum regime. The same concept is used to extract α_{s} from τ decays. Experimental data are used for the evaluation of eq. (8) in the charm–anticharm resonance region beyond the opening of the $D\bar{D}$ threshold.

A significant improvement in the knowledge of the low-energy e^+e^- cross-sections was obtained by realizing [112,113] that the high luminosity available at the modern Φ and B factories made it possible to exploit events with hard initial-state photon radiation to measure the cross-section of the process $e^+e^- \to$ hadrons (s') at any energy $\sqrt{s'}$ below $\sqrt{s}$, the centre-of-mass energy of the experiment. The measurement of the corresponding radiative process is required, where the photon is emitted by the colliding electrons so that $s' = s(1 - 2E_\gamma^\star/\sqrt{s})$, where $E_\gamma^\star$ is the centre-of-mass energy of the radiated photon. Figure 12b shows the $e^+e^- \to \pi^+\pi^-(\gamma)$ cross-section measured by BABAR using

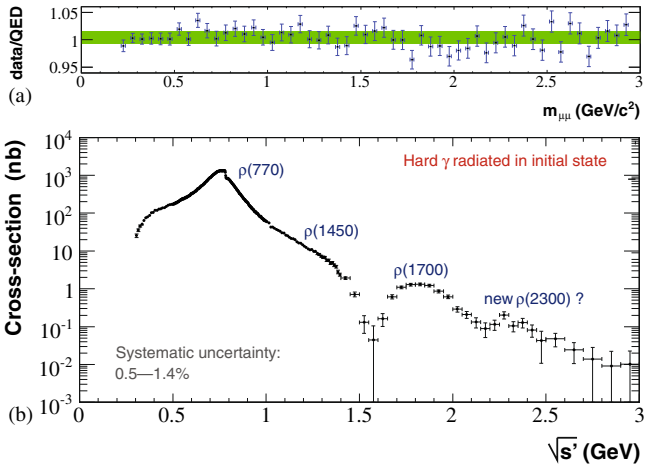

Figure 12. (**a**) Ratio of measured cross-section for $e^+e^- \to \mu^+\mu^-(\gamma)$ to the NLO QED prediction. The band is the result of a fit. It includes statistical and systematic errors. (**b**) Measured cross-section for $e^+e^- \to \pi^+\pi^-(\gamma)$ vs. the effective centre-of-mass energy. The data have been unfolded from detector effects. The various known ρ resonances as well as the ρ–ω mixing edge are clearly visible (figure taken from ref. [114] (modified)).

this technique [114]. The measurement is systematics dominated, with errors ranging between 0.5 and 1.4%. Figure 12a shows the ratio of the $e^+e^- \to \mu^+\mu^-(\gamma)$ cross-section between data and the prediction from QED. Good agreement is observed, demonstrating that all relevant efficencies and acceptance requirements (trigger, photon, tracking, particle identification, kinematic fit, acceptance) are understood. The comparison of different cross-section data [115] revealed a discrepancy between the most precise measurements by BABAR and KLOE [116,117]. In summer 2011, KLOE presented a new preliminary measurement [118] of the two-pion cross-section employing, as was done by BABAR, the $\pi\pi(\gamma)/\mu\mu(\gamma)$ ratio for which radiation, luminosity, and vacuum polarization corrections, as well as several acceptance-related systematic uncertainties cancel. The ratio crucially relies on a well-understood π/μ separation in the detector. The analysis used 239 pb^{-1} of data, giving 3.4(0.9) million $\pi\pi(\gamma)(\mu\mu(\gamma))$ events, and achieved an overall systematic precision of 1%. Good agreement with the previous KLOE results is found so that the observed discrepancy with BABAR is corroborated.

Precise BABAR data available for several higher multiplicity modes with and without kaons help to discriminate between older, less precise and sometimes contradicting measurements. Figure 13 shows as an example the cross-section measurements and their averages for the $e^+e^- \to \pi^+\pi^-2\pi^0$ and $e^+e^- \to K^+K^-\pi^+\pi^-$ channels. In several occurrences, the older measurements overestimate the cross-sections in comparison with BABAR, which contributes to the reduction in the newer evaluations of the hadronic loop effects. The BABAR data also greatly help to improve the estimates of unmeasured modes via isospin constraints from measured ones [115].

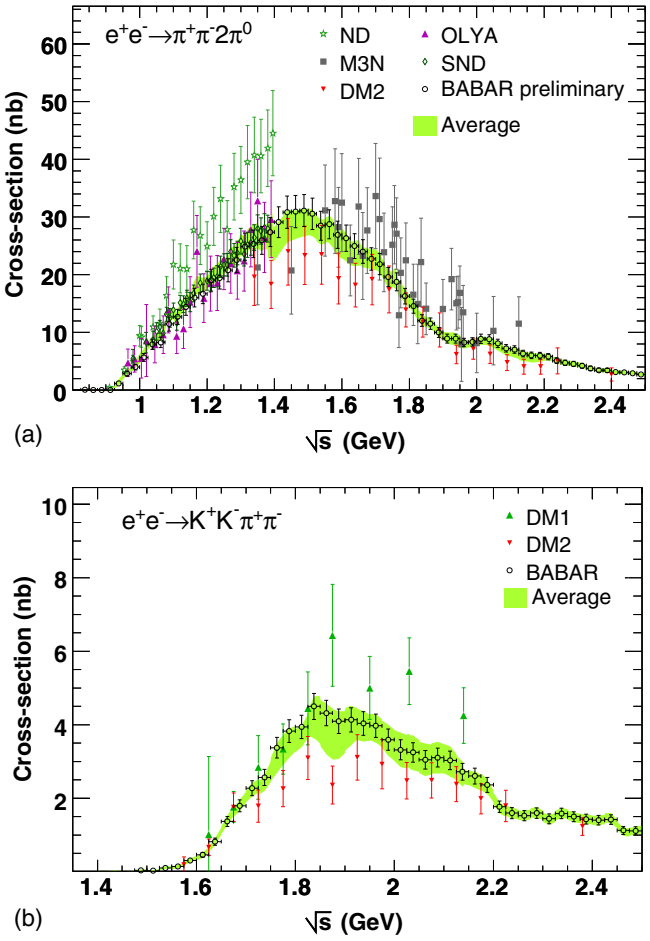

Figure 13. Cross-section data for the e^+e^- final states $\pi^+\pi^-2\pi^0$ (**a**) and $K^+K^-\pi^+\pi^-$ (**b**). The BABAR data [119,120] improve the precision and resolve inconsistencies among earlier datasets (figure taken from ref. [115]).

Summing the contributions from all the available $\sigma(e^+e^- \to \text{hadrons})$ modes and those evaluated with perturbative QCD, the integral (8) gives [115]

$$a_\mu^{\text{had,LO}} = (6923 \pm 42 \pm 3) \cdot 10^{-11}, \tag{9}$$

where the first error is experimental (dominated by systematic uncertainties), and the second due to perturbative QCD. New multihadron data from the BABAR experiment have increased the constraints on unmeasured exclusive final states leading to a small reduction in the hadronic contribution compared to previous evaluations.

Alternatively, one can use precise vector spectral functions from $\tau \to \nu_\tau +$ hadron decays [121] that are related to isovector $e^+e^- \to$ hadron cross-sections by isospin symmetry. The τ data are subject to very different systematic uncertainties compared to the e^+e^- data, thus providing a valuable cross-check. Replacing e^+e^- data in the

two-pion and four-pion channels by the corresponding isospin-transformed τ data, and applying isospin-violating corrections (QED radiative corrections, charged versus neutral meson mass splitting and electromagnetic decays, giving $\Delta a_\mu^{\rm had,LO} = (-3.2 \pm 0.4)\%$) one finds [115]

$$a_\mu^{\rm had,LO} = (7015 \pm 42 \pm 19 \pm 3) \cdot 10^{-11}\ (\tau), \tag{10}$$

where the first error is experimental, the second estimates the uncertainty in the isospin-breaking corrections applied to the τ data, and the third error is due to perturbative QCD. The current discrepancy between the e^+e^- and τ-based determinations of $a_\mu^{\rm had,LO}$ has been reduced to 1.8σ with respect to earlier evaluations. New e^+e^- and τ data from the B-factory experiments BABAR and Belle have increased the experimental information. Re-evaluated isospin-breaking corrections have also contributed to this improvement [122]. BABAR reported good agreement with the τ data in the most important two-pion channel [114]. The remaining discrepancy with the older e^+e^- and τ datasets may be indicative of problems with one or both datasets. It may also suggest the need for additional isospin-violating corrections to the τ data.

Higher order, $\mathcal{O}(\alpha^3)$, hadronic contributions are obtained from dispersion relations using the same $e^+e^- \to$ hadrons data [121,123,124], giving $a_\mu^{\rm had,NLO}[\rm Disp] = (-98.4 \pm 0.6) \cdot 10^{-11}$, along with model-dependent estimates of the hadronic light-by-light scattering contribution [125], $a_\mu^{\rm had,NLO}[\rm LBL]$, motivated by large-$N_{\rm C}$ QCD [126–129]. Following ref. [127], one finds for the sum of the two terms $a_\mu^{\rm had,NLO} = (7 \pm 26) \cdot 10^{-11}$, where the error is dominated by the light-by-light contribution.

Adding all SM contributions gives the e^+e^- data-based SM prediction

$$a_\mu^{\rm SM} = (116\,591\,802 \pm 2 \pm 42 \pm 26) \cdot 10^{-11}, \tag{11}$$

where the errors are due to the electroweak, lowest-order hadronic, and higher-order hadronic contributions, respectively. The difference between experiment and theory, $\Delta a_\mu = a_\mu^{\rm exp} - a_\mu^{\rm SM} = (287 \pm 63 \pm 49) \cdot 10^{-11}$ (with all errors combined in quadrature), represents an interesting but not yet conclusive discrepancy of $\sim 3.6\sigma$. All the recent estimates for the hadronic contribution compiled in figure 14 exhibit similar discrepancies. Switching to τ data reduces the discrepancy to 2.4σ, assuming that the isospin-violating corrections are under control within the estimated uncertainties.

An alternate interpretation is that Δa_μ may be a new physics signal with supersymmetric particle loops. Such a scenario is quite natural, since generically, supersymmetric models predict [78] an additional contribution to $a_\mu^{\rm SM}$ of order

$$a_\mu^{\rm SUSY} \simeq \pm 130 \cdot 10^{-11} \cdot \left(\frac{100\ {\rm GeV}}{m_{\rm SUSY}}\right)^2 \tan\beta\,, \tag{12}$$

where $m_{\rm SUSY}$ is a representative supersymmetric mass scale and $\tan\beta \simeq 3$–40 is a potential enhancement factor. Supersymmetric particles in the mass range of 100–500 GeV could be the source of the deviation Δa_μ. If so, those particles can be directly observed at the next generation of high-energy colliders. New physics effects [78] other than supersymmetry can also explain a non-vanishing Δa_μ. A recent popular scenario involves the 'dark photon', a relatively light hypothetical vector boson from the dark matter sector that couples to our world of particle physics through mixing with the ordinary photon [131,132]. As a result, it couples to ordinary charged particles with strength $\varepsilon \cdot e$

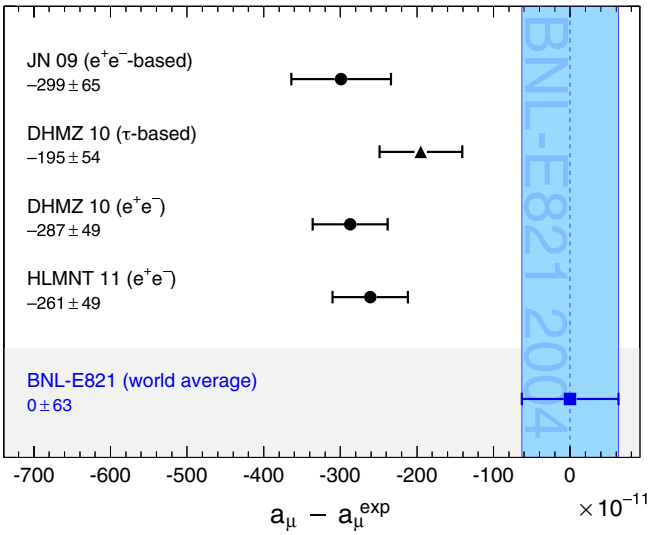

Figure 14. Compilation of recently published results for a_μ (in units of 10^{-11}), subtracted by the central value of the experimental average (6). The shaded band indicates the experimental error. The SM predictions are taken from JN [86], DHMZ [115], and HMNT [123]. Note that the quoted errors do not include the uncertainty on the subtracted experimental value (figure from ref. [130]).

giving rise to an additional muon anomalous magnetic moment contribution $a_\mu^{\text{dark photon}} = (\alpha/2\pi)\cdot\varepsilon^2 F(m_V/m_\mu)$, where $F(x)$ is a monotonously falling function with $F(0.1) = 0.8$, $F(1) = 0.2$. For values of $\varepsilon \sim (1\text{–}2)\cdot 10^{-3}$ and $m_V \sim 10\text{–}100\,\text{MeV}$, the dark photon, which was originally motivated by cosmology, can provide a viable solution to the muon $g-2$ discrepancy. Searches for the dark photon in that mass range are currently underway at Jefferson Lab, USA, and MAMI in Mainz, Germany.

Unfortunately, and despite the significant experimental and theoretical progress, the situation of the muon $g-2$ stays inconclusive. Proposals for new experiments based on different experimental approaches exist at FNAL [133] and J-PARC [134]. The FNAL proposal continues the established magic-γ technique, but with higher proton rate than at BNL and less protons per bunch, a 900 m pion decay line (BNL: 80 m) leading to a smaller pion flash at the muon ring injection, zero-degree muons giving a 5–10 times larger muon yield per proton, and 5–10 times as many muons stored per hour than at the BNL experiment. In addition, improved detectors against signal pile-up, new electronics, and a better shimming to reduce B-field variations should lead to a 2.5(3) times smaller systematic error on the B-field (ω_a). The experiment targets a 20 times better statistical error, and a final systematic error of $1.6\cdot 10^{-10}$. The J-PARC proposal anticipates similar precision without a focussing electric field and hence there is no need to choose a particular magic γ. Ultraslow muons ($p_\mu \sim 2.3$ keV), generated from laser-ionized muonium atoms, are used which have a transverse momentum dispersion that is significantly smaller than the longitudinal momentum, allowing the beam to circulate in the storage ring without the focussing field.

6. Conclusions

All of us are passionately following the LHC experiments in their direct searches for electroweak symmetry-breaking remnants and new physics at the TeV-scale energy frontier. Probing new physics orders of magnitude beyond that scale, and helping to decipher possible TeV-scale new physics discovered at the LHC requires hard work on the intensity and precision frontiers.

Charged leptons offer an important spectrum of possibilities. Charged-lepton flavour violation and electric dipole moment measurements have SM-free signals, and current experiments and mature proposals promise orders of magnitude sensitivity improvement over the state-of-the-art. The muon anomalous magnetic moment may already witness a deviation from the SM. New physics models often strongly correlate all these sectors of paricle physics.

Acknowledgements

The author is grateful to Alessandro Baldini, Swagato Banerjee, Robert Bernstein, Michel Davier, Tim Gershon, Herve Hiu Fai Choi, Yoshitaka Kuno, Alberto Lusiani, Bogdan Malaescu, James Miller, Toshinori Mori, Steven Robertson, Karim Trabelsi, Graziano Venanzoni and Zhiqing Zhang for their help with the preparation of the talk.

References

[1] S L Glashow, J Iliopoulos and L Maiani, *Phys. Rev.* **D2**, 1285 (1970)
[2] LHCb Collaboration, 1112.1600 (2011)
[3] CMS Collaboration: *Phys. Rev. Lett.* **107**, 191802 (2011)
[4] W J Marciano, T Mori and J M Roney, *Annu. Rev. Nucl. Part. Sci.* **58**, 315 (2008)
[5] Heavy Flavor Averaging Group (2010), 1010.1589, http://www.slac.stanford.edu/xorg/hfag/tau/index.html
[6] G Danby, J-M Gaillard, K Goulianos, L M Lederman, N Mistry, M Schwartz and J Steinberger, *Phys. Rev. Lett.* **9**, 36 (1962)
[7] G Feinberg, *Phys. Rev.* **110**, 1482 (1958)
[8] MEGA Collaboration: M Ahmed *et al*, *Phys. Rev.* **D65**, 112002 (2002), hep-ex/0111030
[9] Y Kuno and Y Okada, *Rev. Mod. Phys.* **73**, 151 (2001), hep-ph/9909265
[10] M Raidal *et al*, *Eur. Phys. J.* **C57**, 13 (2008), 0801.1826
[11] R Barbier *et al*, *Phys. Rep.* **420**, 1 (2005), hep-ph/0406039
[12] A Baldini, T Mori *et al*, *The MEG experiment: Search for the* $\mu \to e\gamma$ *decay at PSI*, http://meg.psi.ch/docs
[13] MEG Collaboration: J Adam *et al*, *Nucl. Phys.* **B834**, 1 (2010), 0908.2594
[14] MEG Collaboration: R Sawada, *PoS* **ICHEP2010**, 263 (2010)
[15] MEG Collaboration, *Phys. Rev. Lett.* **107**, 171801 (2011), 1107.5547
[16] L Calibbi, A Faccia, A Masiero and S K Vempati, *Phys. Rev.* **D74**, 116002 (2006), hep-ph/0605139
[17] A Masiero, S K Vempati and O Vives, *Nucl. Phys.* **B649**, 189 (2003), hep-ph/0209303
[18] R Kitano, M Koike, S Komine and Y Okada, *Phys. Lett.* **B575**, 300 (2003), hep-ph/0308021
[19] V Cirigliano, R Kitano, Y Okada and P Tuzon, *Phys. Rev.* **D80**, 013002 (2009), 0904.0957
[20] A Czarnecki, W J Marciano and K Melnikov, *AIP Conf. Proc.* **435**, 409 (1998), hep-ph/9801218

[21] R Kitano, M Koike and Y Okada, *Phys. Rev.* **D66**, 096002 (2002), hep-ph/0203110
[22] SINDRUM II Collaboration: W H Bertl *et al*, *Eur. Phys. J.* **C47**, 337 (2006)
[23] See, e.g., R Bernstein, Pittsburgh Seminar, Feb 2011, http://mu2e.fnal.gov
[24] COMET Collaboration, KEK Report 2009-10 (TDR)
[25] Project-X, FNAL, http://projectx.fnal.gov/
[26] J Pasternak *et al*, *Proc. Int. Particle Accel. Conf. IPAC10* (Kyoto, Japan, 2010)
A Sato *et al*, *Proc. EPAC2006* (Edinburgh, 2006) p. 2508
[27] BABAR Collaboration, *Phys. Rev. Lett.* **104**, 021802 (2010), 0908.2381
[28] Y Miyazaki *et al*, *Phys. Lett.* **B699**, 251 (2011), 1101.0755
[29] SuperB Collaboration, 0709.0451 (2007)
[30] Belle II Collaboration (2010), Long author list - awaiting processing, 1011.0352
[31] K Hayasaka, *J. Phys.: Conf. Series* **171**, 1, 012079 (2009)
[32] T2K Collaboration, *Phys. Rev. Lett.* **107**, 041801 (2011), 1106.2822
[33] J Hisano, M Nagai, P Paradisi and Y Shimizu, *J. High Energy Phys.* **0912**, 030 (2009), 0904.2080
[34] S K Lamoreaux and R Golub, *J. Phys.* **G36**, 104002 (2009)
[35] M Pospelov and A Ritz, *Ann. Phys.* **318**, 119 (2005), hep-ph/0504231
[36] K Kirch, Talk at *PANIC 2011* (MIT-Cambridge, USA)
[37] G Zsigmond, Talk at *EPS-HEP 2011* (Grenoble, France)
[38] C A Baker *et al*, *Phys. Rev. Lett.* **97**, 131801 (2006), hep-ex/0602020
[39] Storage Ring EDM Collaboration, http://www.bnl.gov/edm/
[40] Y Semertzidis, Talk at *Patras-Axion Workshop 2011* (Mykonos, Greece)
[41] B C Regan, E D Commins, C J Schmidt and D DeMille, *Phys. Rev. Lett.* **88**, 071805 (2002)
[42] J J Hudson *et al*, *Nature* **473**, 493 (2011)
[43] L I Schiff, *Phys. Rev.* **132**, 2194 (1963)
[44] J J Hudson, B E Sauer, M R Tarbutt and E A Hinds, *Phys. Rev. Lett.* **89**, 023003 (2002), hep-ex/0202014
[45] ALEPH Collaboration, *Phys. Rep.* **421**, 191 (2005), hep-ex/0506072
[46] Particle Data Group: K Nakamura *et al*, *J. Phys.* **G37**, 075021 (2010)
[47] ALEPH Collaboration, DELPHI Collaboration, L3 Collaboration, OPAL Collaboration, SLD Collaboration, LEP Electroweak Working Group, SLD Electroweak and Heavy Flavour Group, *Phys. Rep.* **427**, 257 (2006), hep-ex/0509008
[48] S Weinberg, *Phys. Rev.* **112**, 1375 (1958)
[49] A Pich, *Phys. Lett.* **B196**, 561 (1987)
[50] S Nussinov and A Soffer, *Phys. Rev.* **D78**, 033006 (2008), 0806.3922
[51] BABAR Collaboration, *Phys. Rev.* **D83**, 032002 (2011), 1011.3917
[52] I I Bigi and A I Sanda, *Phys. Lett.* **B625**, 47 (2005), hep-ph/0506037
[53] Y Grossman and Y Nir, 1110.3790 (2011)
[54] J H Kuhn and E Mirkes, *Phys. Lett.* **B398**, 407 (1997), hep-ph/9609502
[55] BABAR Collaboration, *Phys. Rev.* **D83**, 071103 (2011), 1011.5477
[56] Belle Collaboration, *Phys. Rev. Lett.* **107**, 131801 (2011), 1101.0349
[57] BABAR Collaboration, 1109.1527 (2011)
[58] M Davier, A Hoecker and A Zhang, *Rev. Mod. Phys.* **78**, 1043 (2006), hep-ph/0507078
[59] ALEPH Collaboration, *Z. Phys.* **C76**, 15 (1997)
[60] ALEPH Collaboration, *Eur. Phys. J.* **C4**, 409 (1998)
[61] OPAL Collaboration, *Eur. Phys. J.* **C7**, 571 (1999), hep-ex/9808019
[62] D Boito *et al*, 1112.4202 (2011)
[63] P A Baikov, K G Chetyrkin and J H Kuhn, *Phys. Rev. Lett.* **101**, 012002 (2008), 0801.1821
[64] M Davier, S Descotes-Genon, A Hoecker, B Malaescu and Z Zhang, *Eur. Phys. J.* **C56**, 305 (2008), 0803.0979

[65] M Beneke and M Jamin, *J. High Energy Phys.* **0809**, 044 (2008), 0806.3156
[66] A Menke, 0904.1796 (2009)
[67] I Caprini and J Fischer, *Phys. Rev.* **D84**, 054019 (2011), 1106.5336
[68] T van Ritbergen, J A M Vermaseren and S A Larin, *Phys. Lett.* **B400**, 379 (1997), hep-ph/9701390
[69] K G Chetyrkin, Bernd A Kniehl and M Steinhauser, *Phys. Rev. Lett.* **79**, 2184 (1997), hep-ph/9706430
[70] K G Chetyrkin, B A Kniehl and M Steinhauser, *Nucl. Phys.* **B510**, 61 (1998), hep-ph/9708255
[71] G Rodrigo, A Pich and A Santamaria, *Phys. Lett.* **B424**, 367 (1998), hep-ph/9707474
[72] M Baak *et al*, 1107.0975 (2011)
[73] S Bethke, *Eur. Phys. J.* **C64**, 689 (2009), 0908.1135
[74] K G Chetyrkin and A Kwiatkowski, *Z. Phys.* **C59**, 525 (1993), hep-ph/9805232
[75] Kim Maltman, *Phys. Rev.* **D58**, 093015 (1998), hep-ph/9804298
[76] CKMfitter Group: V Niess, Talk at *EPS 2011* (Grenoble, France), http://ckmfitter.in2p3.fr
[77] This discussion follows in large parts the Review [130]
[78] A Czarnecki and W J Marciano, *Phys. Rev.* **D64**, 013014 (2001), hep-ph/0102122
[79] M Davier and W J Marciano, *Annu. Rev. Nucl. Part. Sci.* **54**, 115 (2004)
[79a] In spite of the breathtaking accuracy of the most recent electron $g-2$ measurement by the Harvard group [80], giving $a_e^{\rm exp} = (11\,596\,521\,807.3 \pm 2.8) \cdot 10^{-13}$, exploiting this measurement to search for new physics is limited by the knowledge of the electromagnetic fine structure constant, α. Inserting independent measurements of α from atom recoil analyses [81–84], effectively reduces the above accuracy by a factor of 20
[80] D Hanneke, S Fogwell and G Gabrielse, *Phys. Rev. Lett.* **100**, 120801 (2008), 0801.1134
[81] P Cladé *et al*, *Phys. Rev. Lett.* **96**, 033001 (2006)
[82] Malo Cadoret *et al*, *Phys. Rev. Lett.* **101**, 230801 (2008), 0810.3152
[83] P Cladé *et al*, *Phys. Rev.* **A74**, 052109 (2006)
[84] V Gerginov *et al*, *Phys. Rev.* **A73**, 032504 (2006)
[85] J P Miller, E de Rafael and B L Roberts, *Rep. Prog. Phys.* **70**, 795 (2007), hep-ph/0703049
[86] F Jegerlehner and A Nyffeler, *Phys. Rep.* **477**, 1 (2009), 0902.3360
[87] Muon g-2: G W Bennett *et al*, *Phys. Rev. Lett.* **89**, 101804 (2002), Erratum, *ibid.* **89**, 129903 (2002), hep-ex/0208001
[88] Muon g-2: G W Bennett *et al*, *Phys. Rev. Lett.* **92**, 161802 (2004), hep-ex/0401008
[89] Muon G-2: G W Bennett *et al*, *Phys. Rev.* **D73**, 072003 (2006), hep-ex/0602035
[90] CERN-Mainz-Daresbury: J Bailey *et al*, *Nucl. Phys.* **B150**, 1 (1979)
[91] Julian S Schwinger, *Phys. Rev.* **73**, 416 (1948)
[92] T Kinoshita and M Nio, *Phys. Rev.* **D73**, 013003 (2006), hep-ph/0507249
[93] T Aoyama, M Hayakawa, T Kinoshita and M Nio, *Phys. Rev. Lett.* **99**, 110406 (2007), 0706.3496
[94] T Kinoshita and M Nio, *Phys. Rev.* **D70**, 113001 (2004), hep-ph/0402206
[95] T Kinoshita and M Nio, *Phys. Rev.* **D73**, 053007 (2006), hep-ph/0512330
[96] A L Kataev, hep-ph/0602098 (2006)
[97] M Passera, *J. Phys.* **G31**, R75 (2005), hep-ph/0411168
[98] G Gabrielse, D Hanneke, T Kinoshita, M Nio and B C Odom, *Phys. Rev. Lett.* **97**, 030802 (2006), Erratum, *ibid.* **99**, 039902 (2007)
[99] R Jackiw and S Weinberg, *Phys. Rev.* **D5**, 2396 (1972)
[100] A Czarnecki, W J Marciano and A Vainshtein, *Phys. Rev.* **D67**, 073006 (2003), Erratum, *ibid.* **D73**, 119901 (2006), hep-ph/0212229

[101] S Heinemeyer, D Stockinger and G Weiglein, *Nucl. Phys.* **B699**, 103 (2004), hep-ph/0405255
[102] T Gribouk and A Czarnecki, *Phys. Rev.* **D72**, 053016 (2005), hep-ph/0509205
[103] A Czarnecki, B Krause and W J Marciano, *Phys. Rev. Lett.* **76**, 3267 (1996), hep-ph/9512369
[104] A Czarnecki, B Krause and W J Marciano, *Phys. Rev.* **D52**, 2619 (1995), hep-ph/9506256
[105] S Peris, M Perrottet and E de Rafael, *Phys. Lett.* **B355**, 523 (1995), hep-ph/9505405
[106] T V Kukhto, E A Kuraev, Z K Silagadze and A Schiller, *Nucl. Phys.* **B371**, 567 (1992)
[107] G Degrassi and G F Giudice, *Phys. Rev.* **D58**, 053007 (1998), hep-ph/9803384
[108] Xu Feng, Karl Jansen, Marcus Petschlies and Dru B Renner, 1103.4818 (2011)
[109] C Bouchiat and L Michel, *Phys. Rev.* **106**, 170 (1957)
[110] M Gourdin and E De Rafael, *Nucl. Phys.* **B10**, 667 (1969)
[111] S J Brodsky and E De Rafael, *Phys. Rev.* **168**, 1620 (1968)
[112] A B Arbuzov, E A Kuraev, N P Merenkov and L Trentadue, *J. High Energy Phys.* **9812**, 009 (1998), hep-ph/9804430
[113] S Binner, J H Kuhn and K Melnikov, *Phys. Lett.* **B459**, 279 (1999), hep-ph/9902399
[114] BABAR Collaboration, *Phys. Rev. Lett.* **103**, 231801 (2009), 0908.3589
[115] M Davier, A Hoecker, B Malaescu and Z Zhang, *Eur. Phys. J.* **C71**, 1515 (2011), 1010.4180
[116] KLOE Collaboration, *Phys. Lett.* **B700**, 102 (2011), 1006.5313
[117] KLOE Collaboration, *Phys. Lett.* **B670**, 285 (2009), 0809.3950
[118] KLOE Collaboration: G Venanzoni, Talk at *EPS-HEP 2011* (Grenoble, France)
[119] BABAR Collaboration: V P Druzhinin, Talk at *the* 23rd *International Symposium on Lepton–Photon Interactions at High Energy (LP07)* (Daegu, Korea, 13–18 Aug 2007) published in Daegu 2007, Lepton and photon interactions at high energies 134, arXiv:0710.3455
[120] BABAR Collaboration, *Phys. Rev.* **D71**, 052001 (2005), hep-ex/0502025
[121] R Alemany, M Davier and A Hoecker, *Eur. Phys. J.* **C2**, 123 (1998), hep-ph/9703220
[122] M Davier *et al*, *Eur. Phys. J.* **C66**, 127 (2010), 0906.5443
[123] K Hagiwara, R Liao, A D Martin, D Nomura and T Teubner, *J. Phys.* **G38**, 085003 (2011), 1105.3149
[124] B Krause, *Phys. Lett.* **B390**, 392 (1997), hep-ph/9607259
[125] Some recent representative estimates of the hadronic light-by-light scattering contribution, $a_\mu^{\mathrm{had,NLO}}$[LBL], that followed after the sign correction of [135,136], are: $(105 \pm 26) \cdot 10^{-11}$ [127], $(110 \pm 40) \cdot 10^{-11}$ [126], $(136 \pm 25) \cdot 10^{-11}$ [128]
[126] J Bijnens and J Prades, *Mod. Phys. Lett.* **A22**, 767 (2007), hep-ph/0702170
[127] J Prades, E de Rafael and A Vainshtein, 0901.0306 (2009)
[128] K Melnikov and A Vainshtein, *Phys. Rev.* **D70**, 113006 (2004), hep-ph/0312226
[129] E de Rafael, *Phys. Lett.* **B322**, 239 (1994), hep-ph/9311316
[130] A Hoecker and W Marciano, *The muon anomalous magnetic moment*, in: Particle Data Group (K Nakamura *et al*), *J. Phys.* **G37**, 075021 (2010)
[131] M Pospelov, *Phys. Rev.* **D80**, 095002 (2009), 0811.1030
[132] D Tucker-Smith and I Yavin, *Phys. Rev.* **D83**, 101702 (2011), 1011.4922
[133] New $g-2$ Collaboration, http://gm2.fnal.gov/public_docs/proposals/Proposal-APR5-Final.pdf
[134] V Vrba *et al*, Report KEK_J-PARC-PAC2009-06
See also, e.g., Naohito SAITO (KEK), Seminar at DESY 2011
[135] M Knecht and A Nyffeler, *Phys. Rev.* **D65**, 073034 (2002), hep-ph/0111058
[136] M Knecht, A Nyffeler, M Perrottet and E de Rafael, *Phys. Rev. Lett.* **88**, 071802 (2002), hep-ph/0111059